EPJ Web of Conferences **276**, 01019 (2023) https://doi.org/10.1051/epjconf/202327601019
SQM 2022

Higher-order moments of net-proton and the QCD phase structure

Ho San Ko[1,*]

[1]1 Cyclotron Road Mailstop 70R0319 Berkeley, CA, 94720, U.S.A.

Abstract. Higher-order cumulants of the conserved quantities and their ratios are powerful tools to study the properties of QGP and explore the QCD phase structure, such as critical point and/or the first-order phase transition boundary. In this proceedings, we present the recent results of the higher-order cumulants and ratios at different collision energies. We compare the results with hadronic transport model, Hadron Resonance Gas model, and QCD thermodynamic calculations and discuss the physics implications. Additionally, we mention the near future cumulant analyses and an initial volume fluctuation issue.

1 Introduction

It has been reported from Lattice QCD calculations that it is an analytic crossover between the QGP and the hadron gas states at vanishing baryonic chemical potential (μ_B) [1] and at the temperature of 156.5 ± 1.5 MeV [2]. A critical point followed by a first-order phase transition at high μ_B is predicted from QCD-based model calculations. For example, see Ref. [3]. We search for the possible signature of the critical point and the first-order phase transition in the QCD phase diagram by scanning the temperature and μ_B. This is done by varying the collision energy [4, 5, 6].

One of the methods for the critical point search is measuring a fluctuation of conserved quantities: net-baryon number, net-charge, and net-strangeness. In this proceedings, we will discuss the net-proton analysis results. The net-proton number is experimentally used as a proxy to the net-baryon number [7, 8]. The moments of the distribution of this quantity are analysed by studying their cumulants.

1.1 Experimental observables

Cumulants from the first to the sixth-order can be written as:

$$\begin{aligned} C_1 &= \langle N \rangle, \\ C_2 &= \langle (\delta N)^2 \rangle, \\ C_3 &= \langle (\delta N)^3 \rangle, \\ C_4 &= \langle (\delta N)^4 \rangle - 3\langle (\delta N)^2 \rangle^2, \\ C_5 &= \langle (\delta N)^5 \rangle - 10\langle (\delta N)^2 \rangle \langle (\delta N)^3 \rangle, \\ C_6 &= \langle (\delta N)^6 \rangle + 30\langle (\delta N)^2 \rangle^3 - 15\langle (\delta N)^2 \rangle \langle (\delta N)^4 \rangle - 10\langle (\delta N)^3 \rangle^2, \end{aligned} \tag{1}$$

*e-mail: h-s.ko@lbl.gov

© The Authors, published by EDP Sciences. This is an open access article distributed under the terms of the Creative Commons Attribution License 4.0 (http://creativecommons.org/licenses/by/4.0/).

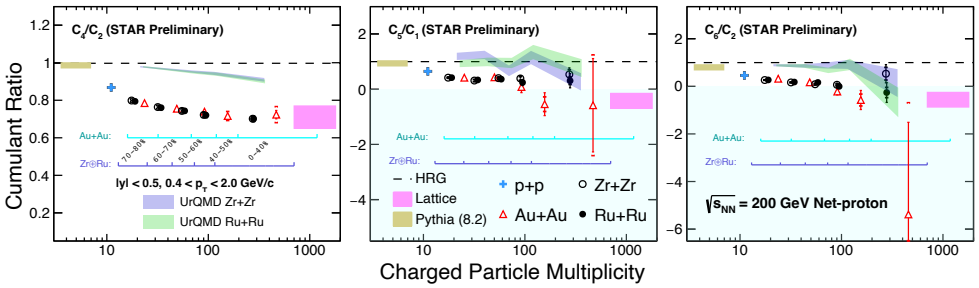

Figure 1: Cumulant ratios C_4/C_2, C_5/C_1, and C_6/C_2 of different collision systems: p+p, ${}^{96}_{40}$Zr+${}^{96}_{40}$Zr, ${}^{96}_{44}$Ru+${}^{96}_{44}$Ru, and Au+Au, as a function of charged particle multiplicity. Cumulant ratios for p+p are presented only in averaged charged particle multiplicity. The detector efficiencies for the charged particle multiplicity are not corrected but corrected for the cumulant ratios. The bars and brackets for each marker represent the statistical and systematic uncertainties, respectively. UrQMD calculations are shown in bands. HRG calculations are shown in dashed lines. Magenta bands represent Lattice QCD prediction for the formation of thermalized QCD matter. Pythia calculations shown in gold bands are for average charged particle multiplicity in p+p collisions.

where N represents the event-by-event conserved quantity distribution and $\delta N = N - \langle N \rangle$. The symbol $\langle N \rangle$ represents the average value of N of the events. The n-th order cumulants are related to the n-th order susceptibility:

$$\chi^{(n)} = \left(\frac{\partial^n p}{\partial \mu_B^n} \right)_T = \frac{1}{VT^3} \times C_n, \tag{2}$$

where p, V, and T represent the pressure, volume, and temperature of the system, respectively. Taking the ratio of the cumulants cancels out the volume dependence and the ratios can be directly compared to theoretical calculations. The higher the cumulant order, the more the cumulant is sensitive to the correlation length [9].

2 Experimental status

From the first principle Lattice QCD calculation, the C_5/C_1 and C_6/C_2 of net-baryon number are expected to be negative [10] where it is a smooth crossover from QGP to hadronic matter. STAR at RHIC measured C_6/C_2 of net-proton number of Au+Au collisions at three different collision energies: 27, 54.4, and 200 GeV [11]. While the results are mostly consistent being zero at other collision energies, the C_6/C_2 progressively become negative as the multiplicity increases and consistent with the Lattice QCD calculation at the most central collision at $\sqrt{s_{\rm NN}} = 200$ GeV.

The same decreasing trend in multiplicity is observed, and presented in figure 1, in the higher-order cumulant ratios C_4/C_2, C_5/C_1, and C_6/C_2 regardless of the collision systems at $\sqrt{s_{\rm NN}}$ =200 GeV: p+p, ${}^{96}_{40}$Zr+${}^{96}_{40}$Zr, ${}^{96}_{44}$Ru+${}^{96}_{44}$Ru, and Au+Au [12, 11]. For better statistics, the collision centralities from 0% to 40% of ${}^{96}_{40}$Zr+${}^{96}_{40}$Zr, ${}^{96}_{44}$Ru+${}^{96}_{44}$Ru and Au+Au collisions are merged into one central collision bin. For p+p collisions, only the averaged values in multiplicity are shown. The decreasing trend in multiplicity makes the results deviate further from the Hadron Resonance Gas (HRG) model calculations in the Grand Canonical Ensemble picture [13, 14]. Due to the effects of decays, the p+p collisions results show below the Grand Canonical Ensemble prediction. Although the hadronic transport model (UrQMD)

[15] describes the overall multiplicity-dependent trend, they overpredict the results. At the most central Au+Au collision results, the results become consistent with the Lattice QCD prediction for the formation of the thermalized QCD matter and smooth crossover transition. PYTHIA 8.2 (Pythia) calculations in figure 1 represent the cumulant ratios averaged over charged particle multiplicity of the p+p collisions. All the higher-order cumulant ratios from Pythia are consistently positive which is inconsistent with the Lattice QCD results in the case of the fifth and the sixth-order.

For collision energy dependence, higher-order cumulant ratios of net-proton in Au+Au collisions from $\sqrt{s_{\rm NN}}$ = 3 to 200 GeV for 0-40% and 50-60% centralities are presented in figure 2 [16]. For C_4/C_2, 0-5% centralities are shown instead of 0-40% [17]. For the 3 GeV results, a fixed Au target was used instead of colliding the two Au nuclei. Due to the experimental setup, the rapidity range is from -0.5 to 0 for the 3 GeV while it is ±0.5 for the others. Various theoretical calculations are described in the figure caption. The analysis results suggest that the cumulant ratios follow the ordering of $C_4/C_2 > C_5/C_1 > C_6/C_2$ in the range of collision energy of $\sqrt{s_{\rm NN}}$ = 7.7 - 200 GeV. At 3 GeV however, the cumulant ratios show a reversed ordering. For 0-40% collision centrality, while C_5/C_1 does not show a systematic dependence on the collision energy, we observe a progressively negative sign with decreasing energy in the case of C_6/C_2 in the range of $\sqrt{s_{\rm NN}}$ = 7.7 - 200 GeV. At 3 GeV, both cumulant ratios become positive. In the case of peripheral collision, 50-60% centrality, all three ratios are non-negative.

The hierarchy is expected from QCD thermodynamic calculations: Lattice QCD [10] and the QCD-based functional renormalization group (FRG) model [18]. They also show increasingly negative C_5/C_1 and C_6/C_2 as the collision energy decreases over a wide range of $\sqrt{s_{\rm NN}}$ = 7.7 - 200 GeV (μ_B = 420 -20 MeV). One must, however, keep in mind the difference between net-baryon from the theoretical calculations and net-proton from the data with experimental acceptance. In contrast, the HRG canonical ensemble (HRG CE) model predictions [14] do not follow the ordering and remain positive up to the sixth-order. The UrQMD expectations are qualitatively consistent with the 50-60% centrality results. Additionally, the reversed ordering of the cumulant ratios is reproduced by the UrQMD calculations at 3 GeV. This suggests that at $\sqrt{s_{\rm NN}}$ = 3 GeV, it is hadronic interaction dominant [16].

In the vicinity of a critical point, the fourth-order cumulant is expected to have a non-monotonic dependence on the collision energy [19, 20, 21, 22]. At STAR, this behavior for net-proton is observed (see the left plot of figure 2) in the collision energy of $\sqrt{s_{\rm NN}}$ = 7.7 - 62.4 GeV with a significance 3.1σ for the 0-5% central Au+Au collisions [6, 12]. Recent analysis of Au+Au collisions at $\sqrt{s_{\rm NN}}$ = 2.4 and 3 GeV at HADES [23] and STAR [17] respectively, show a suppression of net-proton C_4/C_2. The UrQMD reproduces the data at $\sqrt{s_{\rm NN}}$ = 3 GeV indicating that it is hadronic interaction dominant at this energy.

We briefly mention here, two other measurements at $\sqrt{s_{\rm NN}}$ = 3 GeV: anisotropic flow v_2 scaled by its number of constituent quarks [24] and ϕ-meson ratio over kaon [25, 26]. At higher collision energy, the scaled v_2 is positive. The positive v_2 along with the observation of its number-of-constituent-quarks (NCQ) scaling is a strong evidence of the formation of a hydrodynamically expanding QGP phase with partonic degrees of freedom. However at 3 GeV, it becomes negative and the scaling disappears. The 3 GeV result shows that it needs a description from a new equation of state, likely dominated by baryonic interactions. Also, strangeness production in different collision energy shows that it deviates strongly from Grand Canonical Ensemble at 3 GeV and favors Canonical Ensemble model. Also, a transport model describes the datapoint. This additionally indicates a change of medium. These measurements along with the fourth-order cumulants support that at 3 GeV and below, hadronic interaction is dominant.

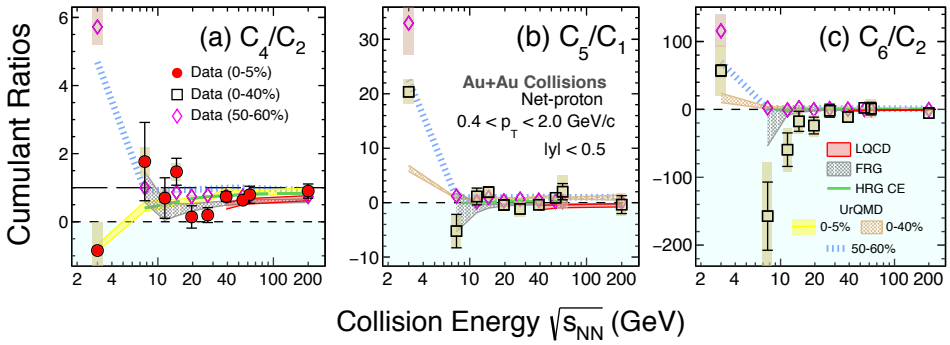

Figure 2: Energy dependence of the net-proton higher-order cumulant ratios of the Au+Au collisions. For C_4/C_2, two collision centralities, 0-5% and 50-60%, are shown while 0-40% and 50-60% are shown for the other cumulant ratios. The rapidity range for $\sqrt{s_{\rm NN}}$ = 3 GeV is from -0.5 to 0 while |y| < 0.5 is used for all other energies. The bars and bands represent the statistical and systematic uncertainties of the data points, respectively. Lattice QCD (39 - 200 GeV), FRG (7.7 - 200 GeV), UrQMD, and HRG CE (7.7 - 200 GeV) are shown as red, grey, brown and blue-dashed bands, and green dashed lines, respectively.

The higher-order cumulant analysis at $\sqrt{s_{\rm NN}}$ = 200 GeV strongly suggests that the thermalized QGP matter is formed and it is a smooth crossover between the QGP and hadron gas states. As the collision energy decreases, the fourth-order cumulant (C_4/C_2) exhibits non-monotonic energy dependence in the collision energy range of $\sqrt{s_{\rm NN}}$ = 7.7 - 62.4 GeV. At 3 GeV and below, it hints a hadronic interaction dominance. Therefore, if the QCD critical point exists, it is likely that it exists between 3 and 200 GeV.

3 Upcoming analyses

As described in equation 2, the n-th order cumulant is the n-th derivative of chemical potential. Therefore, the higher the order, the more cumulant contains the structure of the chemical potential and the more fluctuates to the variation. Cumulants of order higher than the sixth, up to the eighth, are currently under study. However, it needs attentiveness since the higher the order, the more statistic it needs and the more vulnerable to the background.

Analysis of cumulant ratios of mixed quantum numbers may enable us to measure the magnetic field created in heavy-ion collisions [27]. For baryon-strangeness correlation studies, strange baryon measurements become crucial [28]. Therefore, the detection efficiency and purity of the detected particles need to be carefully studied. See Ref. [29] as an example of the purity correction study.

The Phase II of the STAR beam energy scan collected higher statistics, compared to the first phase, on collision energies of $\sqrt{s_{\rm NN}}$ = 7.7 - 27 GeV. The focus of this energy range is to provide the most precise data to map the QCD phase diagram and pin down the critical point. Not only the statistics have been improved, but also the detector upgrades help reduce the systematic uncertainty of the measurement. The addition of the inner TPC (iTPC) to the TPC helps enlarge the acceptance. More rigorous rapidity scan can be performed.

4 Initial volume fluctuation at high baryon density

There are future experimental facilities that are focusing on the high baryon density region, with high statistics: NICA, HADES, HIAF, FAIR, and JPARC-HI. They will map out the

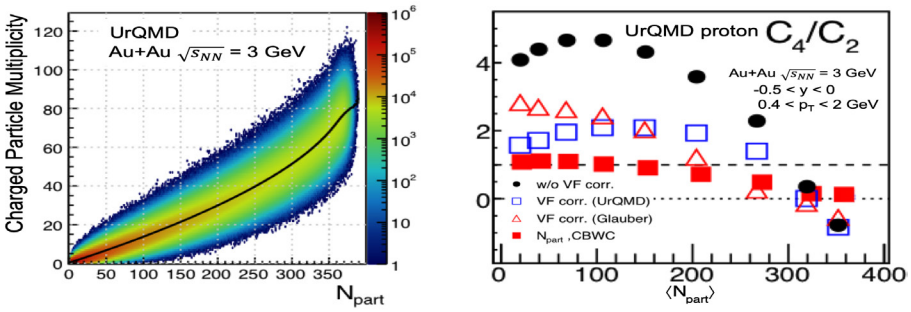

Figure 3: UrQMD model calculations. Left: charged particle multiplicity to N_{part} of Au+Au collisions at $\sqrt{s_{NN}}$ = 3 GeV. Right: C_4/C_2 of the proton to $\langle N_{part} \rangle$ of Au+Au collisions at $\sqrt{s_{NN}}$ = 3 GeV. Black dots represent the cumulant ratios calculated using the charged particle multiplicity. Red squares show when using the N_{part} for the calculation. The blue squares and the red triangles indicate the results using the charged particle multiplicity with initial volume fluctuation (IVF) corrections applied. Different model-based IVF corrections are applied for the blue squares and the red triangles results.

QCD phase diagram above the high baryon density region covered by RHIC. One of the challenges these facilities need to face is an initial volume fluctuation (IVF) issue.

We convert the charged particle multiplicity to the collision centrality or the number of participating nucleons (N_{part}) via a Glauber model coupled with a two-component particle production model. This method works well at the LHC energy and high RHIC energy, i.e. low baryon density region. However, as the collision energy decreases, the number of produced particles reduces. The plots in figure 3 are from the UrQMD model study. The left plot shows the charged particle multiplicity to N_{part} of Au+Au collisions at $\sqrt{s_{NN}}$ = 3 GeV. Comparing the case of the charged particle multiplicity at 40 and to 100, for example, one can see that the corresponding range of N_{part} drastically increases. The non-one-to-one correspondence between the two is the IVF and it is more significant in the mid-central collisions due to no constraints by the minimum N_{part} = 0 nor the maximum N_{part} = 394. We find that IVF is significant for $\sqrt{s_{NN}}$ < 7.7 GeV and further studies are ongoing.

The right plot of figure 3 shows the C_4/C_2 of proton of Au+Au collisions at $\sqrt{s_{NN}}$ = 3 GeV. Using the traditionally obtained charged particle multiplicity gives different results from the ideal case of using the N_{part}. The difference is the largest for the mid-central collisions. This is because for the mid-central collisions, the IVF is the most enhanced as described above. In contrasts, the IVF is less significant for the most-central collisions due to the constraints of the maximum N_{part} = 394. The IVF corrections show model dependence. If one could measure the N_{part} independently, it would provide an additional constraints suppressing the IVF effect on the measured cumulants.

5 Summary

The cumulant analysis of conserved quantities probes the QCD phase structure. We presented in this proceedings the higher-order net-proton cumulant analysis results for different systems and energy range. At $\sqrt{s_{NN}}$ = 200 GeV, we showed that the thermalized QGP is formed at the most central Au+Au collisions and it is an analytic crossover to the hadronic matter. In $\sqrt{s_{NN}}$ = 7.7 - 200 GeV, the higher-order cumulant ratios of the central collisions are mostly consistent with the QCD thermodynamic calculations. We also observed the non-monotonic energy dependence of the fourth-order in the range of $\sqrt{s_{NN}}$ = 7.7 - 62.4 GeV hinting that we

are at the vicinity of the critical point. Additionally, we presented that at $\sqrt{s_{\rm NN}}$ = 3 GeV, it is hadronic interaction dominant, implying that if the QCD critical point is created in heavy-ion collision, it likely exists at above 3 GeV. The upcoming experiments will provide better controlled systematic uncertainties and higher statistics to finely map out the QCD diagram to pin down the critical point. The cumulant analysis of mixed quantum numbers may allow us to measure the magnetic field created in heavy-ion collisions. In the high baryon density region, the initial volume fluctuation issue remains and needs to be dealt with.

References

[1] Y. Aoki et al. Nature 443 (2006), pp. 675–678.
[2] A. Bazavov et al., HotQCD. Phys. Lett. B 795 (2019), pp. 15–21.
[3] M. A. Halasz et al. Phys. Rev. D 58 (1998), p. 096007.
[4] Chi Yang. Nucl. Phys. A 967 (2017), pp. 800–803.
[5] L. Adamczyk et al., STAR. Phys. Rev. C 96.4 (2017), p. 044904.
[6] J. Adam et al., STAR. Phys. Rev. Lett. 126.9 (2021), p. 092301.
[7] Y. Hatta and M. A. Stephanov. Phys. Rev. Lett. 91 (2003). [Erratum: Phys.Rev.Lett. 91, 129901 (2003)], p. 102003.
[8] M. Kitazawa and M. Asakawa. Phys. Rev. C 86 (2012). [Erratum: Phys.Rev.C 86, 069902 (2012)], p. 024904.
[9] M. A. Stephanov. Phys. Rev. Lett. 102 (2009), p. 032301.
[10] A. Bazavov et al. Phys. Rev. D 101.7 (2020), p. 074502.
[11] M. S. Abdallah et al., STAR. Phys. Rev. Lett. 127.26 (2021), p. 262301.
[12] M. S. Abdallah et al., STAR. Phys. Rev. C 104.2 (2021), p. 024902.
[13] P. Garg et al. Phys. Lett. B 726 (2013), pp. 691–696.
[14] P. Braun-Munzinger et al. Nucl. Phys. A 1008 (2021), p. 122141.
[15] M. Bleicher et al. J. Phys. G 25 (1999), pp. 1859–1896.
[16] STAR. arXiv: 2207.09837v1 [nucl-ex].
[17] M. S. Abdallah et al., STAR. Phys. Rev. Lett. 128.20 (2022), p. 202303.
[18] Wei-jie Fu et al. Phys. Rev. D 104.9 (2021), p. 094047.
[19] M. A. Stephanov. Phys. Rev. Lett. 107 (2011), p. 052301.
[20] B. J. Schaefer and M. Wagner. Phys. Rev. D 85 (2012), p. 034027.
[21] J.-W. Chen et al. Phys. Rev. D 93.3 (2016), p. 034037.
[22] J.-W. Chen et al. Phys. Rev. D 95.1 (2017), p. 014038.
[23] J. Adamczewski-Musch et al., HADES. Phys. Rev. C 102.2 (2020), p. 024914.
[24] M. S. Abdallah et al. Phys. Lett. B 827 (2022), p. 137003.
[25] J. Adamczewski-Musch et al. Phys. Lett. B 778 (2018), pp. 403–407.
[26] M. S. Abdallah et al. Phys. Lett. B 831 (2022), p. 137152.
[27] H. -T. Ding et al. Eur. Phys. J. A 57.6 (2021), p. 202.
[28] Zhenzhen Yang, Xiaofeng Luo, and Bedangadas Mohanty. Phys. Rev. C 95.1 (2017), p. 014914.
[29] Toshihiro Nonaka. Nucl. Instrum. Meth. A 1039 (2022), p. 167171.